

Off-board Visual Odometry and Control of an Ultralight Quadrotor MAV

Kun Li*, Rui Huang, Swee King Phang, Shupeng Lai, Fei Wang, Ping Tan, Ben M. Chen and Tong Heng Lee
Department of Electrical and Computer Engineering, NUS, Singapore, 117576

ABSTRACT

In this paper, we propose an approach to autonomously control a quadrotor micro aerial vehicle (MAV). With take-off weight of 50 g and 8-min flight endurance, the MAV platform codenamed ‘KayLion’ developed by the National University of Singapore (NUS) is able to perform autonomous flight with pre-planned path tracking. The vision-based autonomous control is realized with a light weight camera system and an ultrasonic range finder integrated to the MAV. An optical flow algorithm is adopted and processed on ground control station to provide position and velocity estimation of the MAV. A model-based position controller is implemented to realize autonomous flight.

1 INTRODUCTION

The rapid development in the area of unmanned aerial vehicles (UAVs) has seen breakthrough and advancement of small-scaled aerial vehicles. These small-scaled air vehicles could be used as scouts in many dangerous civil and military missions, especially showing their superiority in cluttered and constrained indoor environments [1, 2, 3]. Moreover, along with the progress of microchip and microelectromechanical systems (MEMS) technologies, the size of the UAVs have been scaled down to centimeter level. As an example, a palm-sized gliding MAV developed by Harvard University [4], weighing 2 g and 10 cm in length, is capable of autonomous flight target sensing and obstacle avoidance with an optical flow sensor. Another example is Robobee [5], a flapping wing platform created by the same research group. It is only 83 mg and is capable of lift off with external power and execute open-loop pitching and rolling maneuvers. Despite the fact that the platform is only able to fly within a certain distance from the power supply, it is a breakthrough in miniature aerial vehicles.

The term “optical flow” [6] is a bio-inspired concept. It relates to the pattern of apparent motion of objects, surfaces and edges in a visual scene caused by the relative motion between an observer, which is a mono-camera in this case, and the scene. The optical flow method is essential to navigation strategy of MAV due to the poor performance of the

low-cost MEMS GPS sensor signal, or even in indoor environments without GPS. In [7], an optical flow based technique is adopted in outdoor navigation to aid GPS and INS measurement. [8, 9, 10] demonstrated feasible approaches to autonomous MAV navigation and localization in GPS-denied environments with optical flow based motion estimation. The MAV is able to perform autonomous flight in unknown environment with all the algorithms running onboard, while this is not applicable to the ultra-light platforms as described in this paper. In the work done by TU Delft [11], Delfly, a flapping-wing platform with 16 g gross weight including sensors, microcontroller and analog camera, achieved autonomous flight indoor. These works serve as excellent examples to illustrate feasible approaches for indoor and GPS-denied environment navigation, especially implemented for MAV.

This work is an extension of our previous work [12] with vision-based position control and path following. Section 2 discusses the hardware selection, design and assembly with detail specifications. In Section 3, an optical flow based algorithm for motion estimation is presented. Section 4 gives the design methodology of inner-loop and outer-loop control along with the path generation, followed by flight test results provided in Section 5. Concluding remarks are made in Section 6.

2 PLATFORM DESIGN

In this section, a brief introduction of both the hardware design of quadrotor platform and the closed-loop autonomous control will be presented.

2.1 Quadrotor Platform

Our previous work [12] described an explicit methodology to design the quadrotor MAV platform, including mechanical analysis and design, electrical design and assembly as well as test-bench experiments for parameter identification. As shown in Fig. 1a, the quadrotor MAV codenamed ‘KayLion’, weighing 44 g and 15 cm of the diagonal length, consists of a bare quadrotor frame, an attitude and heading reference system (AHRS), as well as a 360 mAh Lithium-Polymer (Li-Po) battery. The system is orientation-stabilized by its onboard inertial measurement unit (IMU) feedback control, with an updating rate of 100 Hz.

In the block ‘UAV’ in Fig. 2, structure of the quadrotor MAV avionic system is displayed. The micro processor Atmega328p receives signals from the 2.4 GHz receiver, angle and angular measurements from the AHRS system and

*Email address: kunli89@nus.edu.sg



(a) Platform with VICON markers (b) Platform with video system

Figure 1: Quadrotor MAV platform codenamed ‘KayLion’

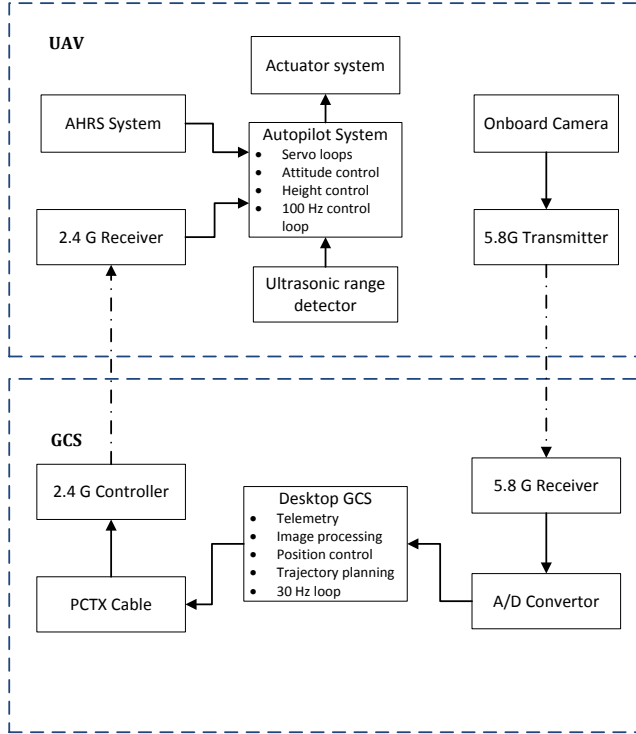


Figure 2: Autonomous control loop hardware architecture

output pulse-width modulation (PWM) signals to four electrical speed controllers (ESCs) to actuate the system.

2.2 Autonomous Control Architecture

Due to limited payload of the quadrotor MAV, there is no weight budget for high power processing units. Thus, the ground control station (GCS) is indispensable for the closed-loop control. Fig. 2 shows the overall architecture of the autonomous UAV, including the orientation stabilization and the position control.

2.2.1 Camera Design

A camera system consisting of an analog camera, an analog transmitter and a 40 mAh Li-Po battery to provide an 8 min flight is customized. Table 1 lists the specifications of the analog camera. The specifications of the analog video trans-

Table 1: Specifications of camera shown in Fig. 3a

Descriptions	Specs
Weight (<i>g</i>)	2
Resolution	704×576
Pixel amount	400000
Lens (<i>mm</i>)	2.78
Power supply (<i>V</i>)	3.5 - 5
View angle	62°

Table 2: Specs of video transceiver shown in Fig. 3b

Descriptions	Transmitter	Receiver
Module	TX5813	RX5808
Weight (<i>g</i>)	3.4	6.5
Frequency range (MHz)	5705-5945	5705-5945
Power supply (<i>V</i>)	3.5-5	3.5-5
Dimension (<i>mm</i>)	$22 \times 20 \times 3$	$28 \times 23 \times 3$

mitter and receiver are highlighted in Table 2. A 40 mAh capacity Li-Po battery was selected to provide sufficient power supply to the camera system. They are integrated on a single customized printed circuit board (PCB) for easy mounting on the platform. Experiment shows that the battery is able to power the system for more than 8 minutes. Fig. 3a shows the mini analog camera, Fig. 3b displays the transceiver combo, Fig. 3c shows the battery and Fig. 3d shows the integrated video system.

2.2.2 Ultrasonic Sonar Sensor

In order to maintain the aircraft at a certain height to perform stable indoor navigation, an ultrasonic sensor, Maxsonar EZ4, is adopted to provide altitude measurement. This sensor provides accurate readings from 0.15 m to 7.65 m with 1 cm resolution and can be powered with 3.3 V power supply. In Fig. 2, ultrasonic sensor is connected to the onboard avionic system via an analog-to-digital port. The overall assembly is presented in Fig. 1b, where the ultrasonic sensor locates in the center of the platform facing downward and the camera locates at rear side also facing downward.

2.2.3 PCTx Connector

For the data-link solution, PCTx cable (see Fig. 4a), connecting the GCS to the RF controller, is a simple approach to meet the closed-loop control without adding extra wireless modules to the MAV. The cable provides 9 channel communication of 50 Hz pulse-position modulation (PPM) signal with 1024 steps resolution. The PCTx cable is able to transmit

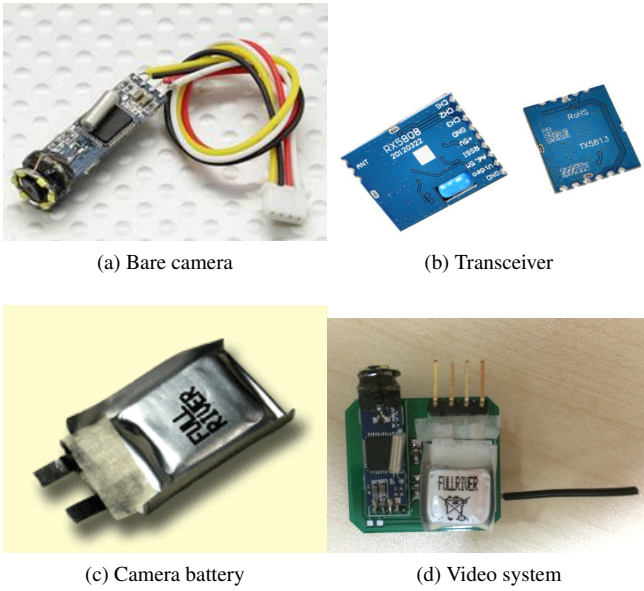


Figure 3: Components for video system

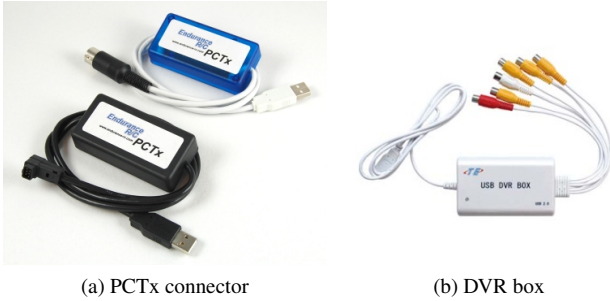


Figure 4: Components for autonomous control

controlled signal generated by the GCS to the aircraft through the RF transmitter.

2.2.4 A/D converter

As indicated in Fig. 2, since the GCS cannot process analog video, a digital video recorder (DVR) (see Fig. 4b) is used to connect the receiver RX5808 to the GCS. The DVR box sends processed digital video signals to GCS via a USB port. A driver program for DVR box is installed on GCS to capture the digital video signal for image processing. The image resolution is set to be 704×576 pixels.

3 MOTION ESTIMATION USING OPTICAL FLOW

Optical flow is a well known algorithm in computer vision society to estimate the 2 dimensional (2-D) motion of features between two consecutive images. By examining the results of optical flow, we can further infer the 3 dimensional (3-D) motion of the camera. Optical-flow-based motion estimation is more memory efficient, compared to a full 3-D

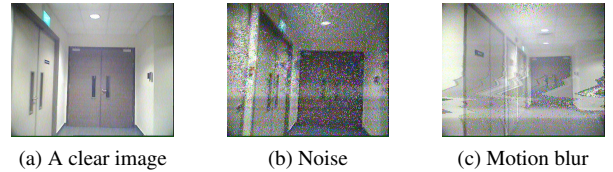


Figure 5: Images affected by transmission noise and motion blur

reconstruction approach such as a visual SLAM system [13] which maintains a full 3-D map and feature tracks. Only the matched features between two consecutive frames need to be maintained in the proposed approach. To improve the computational speed, we downsize the image to 1/4 of the original resolution. Optical flow is further computed for a limited number of sparse feature points so that the system can run in real time at 25 Hz. Moreover, due to the severe transmission interference and motion blur in the video shown in Fig. 5, the feature tracking of the visual SLAM approach [13] might not work well. However, no feature tracks are needed in our case and false estimation due to images of low quality can be easily detected and then rejected. This makes optical-flow-based approach a suitable solution for motion estimation of the current platform.

In this section, we propose an approach to estimate the self motion of the quadrotor MAV equipped with a downward-looking camera via optical flow in an indoor environment.

3.1 Feature Detection and Homography Estimation

Firstly, feature points are detected using Shi-Tomasi feature detector [14]. The features are then tracked over consecutive frames using the Pyramid version of the Lukas-Kanade tracker [15]. In order to achieve high computational speed, we limit the maximum number of detected features to 100. Since the floor of the navigation area is poorly textured, we placed some random markers on the ground to provide sufficient features.

Given the corresponding feature points detected in consecutive frames, the perspective transformation between the two camera frames can be estimated. This transformation is represented by a 3×3 homography matrix. The locations of corresponding feature points \mathbf{p} and \mathbf{p}' in images captured at t and t' are related by the homography matrix as equation 1. \mathbf{p} and \mathbf{p}' are denoted as homogeneous coordinates.

$$s\mathbf{p} = \mathbf{H}\mathbf{p}' \quad (1)$$

According to [16], this relation is satisfied provided that the image scenes lie on the same plane. This assumption can be safely made in our case since all the captured scenes belong to the flat floor. The homography matrix \mathbf{H} can be solved using a standard least square optimization algorithm. RANSAC [17] can be applied to reject outliers for a robust

estimation. The estimated homography is then refined using Levenberg-Marquardt optimization to further reduce the re-projection error. The homography matrix is estimated up to a scale s . Thus it needs to be normalized so that the element in homography matrix $\mathbf{H}_{33} = 1$.

3.2 Self Motion Estimation

As presented in [18], the homography matrix can be further decomposed as the following equation:

$$\mathbf{H} = \mathbf{R} + \frac{1}{d}\mathbf{T}\mathbf{N}^T \quad (2)$$

where \mathbf{R} and \mathbf{T} are the rotation and translation of the UAV frame from t to t' . \mathbf{N} is the unit normal vector of the ground plane at t and d is the distance between the ground plane and the UAV frame. If we can obtain UAV attitude angles ϕ, θ, ψ at t and ϕ', θ', ψ' at t' , \mathbf{N} can then be expressed as

$$\mathbf{N} = \begin{pmatrix} -\sin \theta \\ \sin \phi \cos \theta \\ \cos \phi \cos \theta \end{pmatrix} \quad (3)$$

The rotation \mathbf{R} can be computed as follows,

$$\mathbf{R} = \mathbf{R}_{b/n}(t)\mathbf{R}_{n/b}(t') \quad (4)$$

where $\mathbf{R}_{b/n}(t)$ is the rotation from the UAV body frame to the inertia frame at t and $\mathbf{R}_{n/b}(t')$ is the rotation from the inertia frame to the UAV body frame at t' . Therefore, the translation \mathbf{T} can be calculated as

$$\mathbf{T} = d(\mathbf{H} - \mathbf{R})\mathbf{N} \quad (5)$$

For general cases, we need the measurements from the IMU to calculate the \mathbf{R} and \mathbf{N} . However, since the MAV is moving slowly during the navigation, it has negligible rotation. Thus we can safely assume that \mathbf{R} is an identity matrix and \mathbf{N} is the perpendicular vector to the ground plane. Also the distance between the ground plane and the MAV is measured by an ultrasonic sensor. As the translation \mathbf{T} is estimated, the velocity vector \mathbf{v} of MAV body frame can be computed by,

$$\mathbf{v} = \frac{\mathbf{T}}{\Delta t} \quad (6)$$

where $\Delta t = t' - t$.

3.3 Linear Kalman Filter

We further design a simple linear Kalman Filter to estimate the position of the MAV. The measurement is the estimated velocity based on the homography. The linear state space includes the position and velocity of the MAV,

$$\mathbf{x}_k = \begin{pmatrix} x \\ \dot{x} \end{pmatrix} \quad (7)$$

The state \mathbf{x} is evolved according to the prediction model,

$$\mathbf{x}_k = \mathbf{F}_k\mathbf{x}_{k-1} + \mathbf{B}_k\mathbf{u}_k + \mathbf{w}_k \quad (8)$$

where

$$\mathbf{F}_k = \begin{bmatrix} 1 & \Delta t \\ 0 & 1 \end{bmatrix} \quad (9)$$

and

$$\mathbf{B}_k = \begin{pmatrix} \frac{\Delta t^2}{2} \\ \Delta t \end{pmatrix} \quad (10)$$

and \mathbf{u}_k is the system input which is the MAV acceleration. We assume that the MAV undergoes a constant acceleration which follows a zero mean normal distribution. \mathbf{w}_k is the process noise which follows $N(0, \mathbf{Q}_k)$.

The measurement model is,

$$\mathbf{z}_k = \mathbf{G}_k\mathbf{x}_k + \mathbf{v}_k \quad (11)$$

where

$$\mathbf{G}_k = \begin{pmatrix} 0 & 1 \end{pmatrix} \quad (12)$$

and \mathbf{v}_k is measurement noise which follows $N(0, \mathbf{R}_k)$.

The optical flow algorithm will sometimes fail if the received image is badly affected by motion blur and signal interference during the transmission. However, the failed cases can be detected and discarded before the Kalman filter is updated. Only the estimated velocities between v_{\min} and v_{\max} are used as measurements for the Kalman filter. In our implementation, we set $v_{\min} = 10^{-6}$ m/s and $v_{\max} = 2$ m/s. While the filter is updated only with the valid measurements, it predicts the states at a constant frequency using the prediction model.

4 CONTROL SYSTEM DESIGN

Control methodology of the quadrotor MAV includes three major parts: inner-loop control, outer-loop control and reference generation, which is displayed in Fig. 6. The inner-loop control stabilizes the orientation of the system while the outer-loop control deals with the position, velocity and acceleration of the MAV in the north-east-down (NED) frame. The inner-loop dynamics, which is the part in the blue box in Fig. 6, will not be discussed here since in the previous work, the control strategies of orientation stabilization are investigated with the implementation of linear quadratic regulator (LQR) control law [19].

4.1 Position Control with Optical Flow

A position controller is designed and implemented with Robust and Perfect Tracking (RPT) method, which can be viewed in Fig. 6. As described in Fig. 2, the outer-loop control is realized by two parts: onboard height control with ultrasonic sensor measurement and GCS 2-D position control with optical flow based motion estimation. This control scheme is verified with a high-precision motion capture system VICON, which was discussed in [19] with flight test results.

In terms of RPT position control, the closed inner-loop can be treated as a virtual actuator (see [20]), the outer-loop

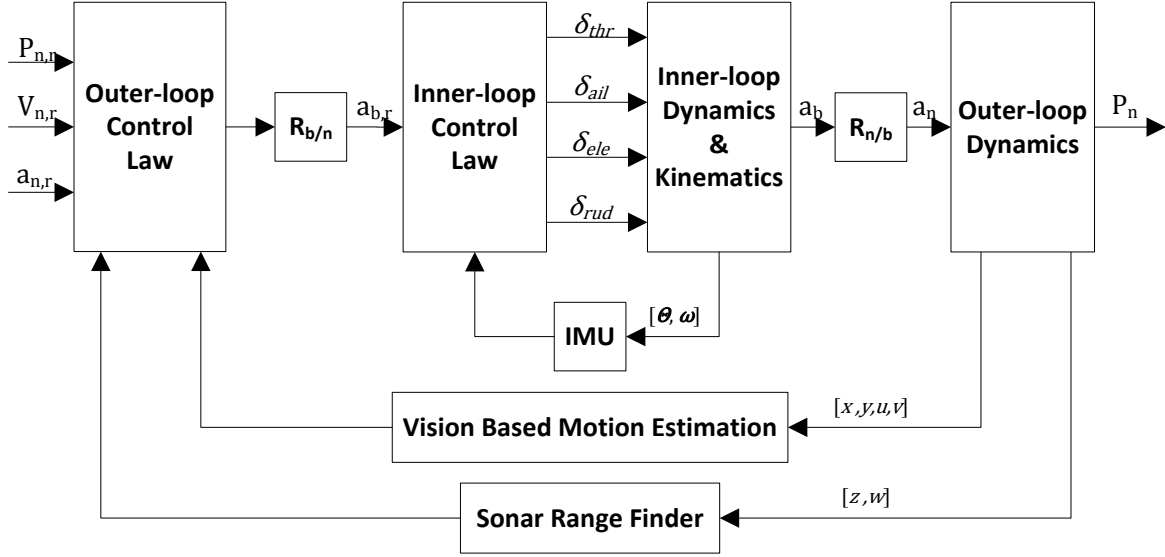


Figure 6: Structure of quadrotor MAV control system

dynamics of the aircraft can be regarded as the dynamics of a universal 6 degree-of-freedom (DoF) particle, without considering the coupling effect, which can be expressed as below:

$$\begin{pmatrix} \dot{x}_n \\ \dot{u}_n \end{pmatrix} = \begin{bmatrix} 0 & 1 \\ 0 & 0 \end{bmatrix} \begin{pmatrix} x_n \\ u_n \end{pmatrix} + \begin{bmatrix} 0 \\ 1 \end{bmatrix} a_{x,n} \quad (13)$$

where x_n , u_n , $a_{x,n}$ are respectively position, velocity and acceleration for x directions in the NED frame. By applying the RPT approach introduced in [21], we can obtain an augmented system of the following form:

$$\Sigma_{\text{AUG}} : \begin{cases} \dot{\mathbf{x}} &= \mathbf{A}\mathbf{x} + \mathbf{B}\mathbf{u} + \mathbf{E}\mathbf{w} \\ \mathbf{y} &= \mathbf{x} \\ \mathbf{h} &= \mathbf{C}_2\mathbf{x} \end{cases} \quad (14)$$

where

$$\mathbf{x} = \begin{pmatrix} \int x_e \\ x_{n,r} \\ u_{n,r} \\ a_{x,n,r} \\ x_n \\ u_n \end{pmatrix} \quad \mathbf{w} = \dot{a}_{x,n,r} \quad (15)$$

with $x_e = x_{n,r} - x_n$ as the position error and $\dot{a}_{x,n,r}$ as the derivative of the acceleration. By following the procedures in [22], a linear feedback control law can be formulated as:

$$\mathbf{u} = \mathbf{F}\mathbf{x}, \quad (16)$$

with

$$\mathbf{F} = \begin{pmatrix} \frac{k_i \omega_n^2}{\epsilon^3} \\ \frac{\omega_n^2 + 2\zeta \omega_n k_i}{\epsilon^2} \\ \frac{2\zeta \omega_n + k_i}{\epsilon} \\ 1 \\ -\frac{\omega_n^2 + 2\zeta \omega_n k_i}{\epsilon^2} \\ -\frac{2\zeta \omega_n + k_i}{\epsilon} \end{pmatrix}^T \quad (17)$$

where ϵ is the design parameter to adjust the settling time of the closed-loop system, ω_n , ζ and k_i are respectively the nominal natural frequency, damping ratio and desired pole location of the closed-loop system of the system (14),

$$p_i(s) = (s + k_i)(s^2 + 2\zeta \omega_n s + \omega_n^2) \quad (18)$$

The parameter ϵ is designed as a small number to achieve fast response. However, due to the limitation of MAV dynamics, the outer-loop bandwidth is chosen as smaller than 1/3 of the inner-loop bandwidth [23].

4.2 Path Generation

In Fig. 6, a smooth reference trajectory in NED frame inclusive of position $P_{n,r}$, velocity $V_{n,r}$ and acceleration $a_{n,r}$ is generated. In cooperation with the control and localization algorithm, a reference trajectory with continuous and limited velocity and acceleration is preferred. It prevents spikes in control input and helps the localization algorithm to achieve a stable and smooth performance. In this paper, a B-spline

based optimization algorithm is adopted to generate a C_2 continuous trajectory whose derivatives are well constrained. A similar method was adopted in the paper [24], except in this application we used one non-linear programming instead of the two layer of quadratic programming. A general form of B-spline is described in [25] as:

$$\begin{aligned} C(\mu) &= \sum_{i=0}^n N_{i,p}(\mu) P_i \\ \mu &= [\mu_0, \mu_1, \mu_2, \dots, \mu_n] \end{aligned} \quad (19)$$

where $C(\mu)$ denotes the reference trajectory, $N_{i,p}(\mu)$ is the basis function and P_i is the control point acquired from user input. The derivative of the B-spline is given as:

$$\begin{aligned} \frac{d}{d\mu} C(\mu) &= \sum_{i=0}^{n-1} N_{i+1,p-1}(\mu) Q_i \\ Q_i &= \frac{p}{\sum_{j=i+1}^{i+p+1} T_j} (P_{i+1} - P_i) \end{aligned} \quad (20)$$

where $T_j = \mu_j - \mu_{j-1}$ is the time segment and Q_i is the control point of the first order derivative. In order to obtain a time optimal trajectory, the overall time span of the trajectory is made as short as possible. Thus, the following optimization problem could be formulated:

$$\begin{aligned} \min \sum T_j^2 & \quad \text{subject to} \\ V_{\min} & \leq Q_i = \frac{p}{\sum_{j=i+1}^{i+p+1} T_j} (P_{i+1} - P_i) < V_{\max} \\ a_{\min} & \leq R_i = \frac{p-1}{\sum_{j=i+1}^{i+p+1} T_j} (Q_{i+1} - Q_i) < a_{\max} \end{aligned} \quad (21)$$

where R_i is the control point of the second derivative and $V_{\max}, V_{\min}, a_{\max}, a_{\min}$ are the upper and lower bounds for velocity and acceleration correspondingly. According to [26], the inequality constraints in (21) serve as the sufficient condition to limit the whole trajectory's velocity and acceleration within any user specified range. Problem in (21) could be solved easily using off-the-shelf non-linear programming package such as *fmincon* from Matlab.

5 EXPERIMENTAL RESULTS

In this section, flight tests are carried out to verify the control methods with our motion estimation algorithm. With the path generator mentioned in the last section, a path along a 2×2 m square was generated. Since the measurements of the ultrasonic sensor cannot be obtained at the GCS, the platform is maintained at 0.75 m height to provide the scale reference to the motion estimation. Fig. 7 shows the 3-D plot of the tracking performance. Fig. 8 presents the comparison between the measurements and references in x and y directions of the inertia frame respectively. To verify the performance of the height control, the measurements of the ultrasonic sensor is recorded onboard. The result is presented in Fig. 9. To further demonstrate the autonomy of our platform, a path along

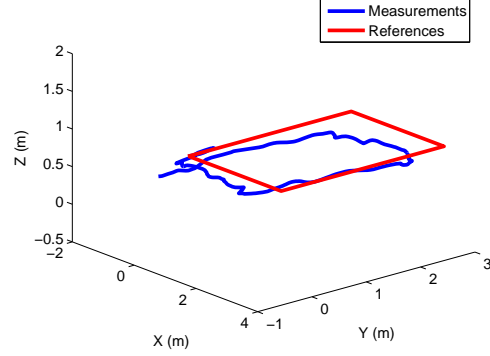


Figure 7: Autonomous flight of a square path

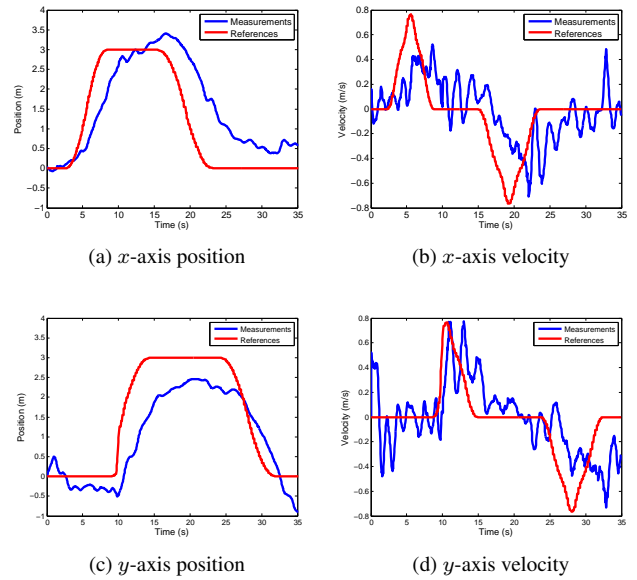


Figure 8: Tracking performance along x and y axes of the square path

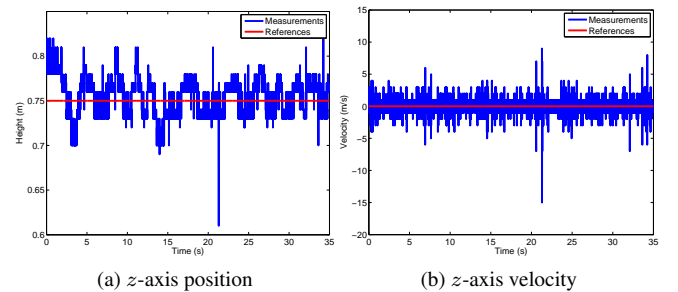


Figure 9: Tracking performance along z axis of the square path

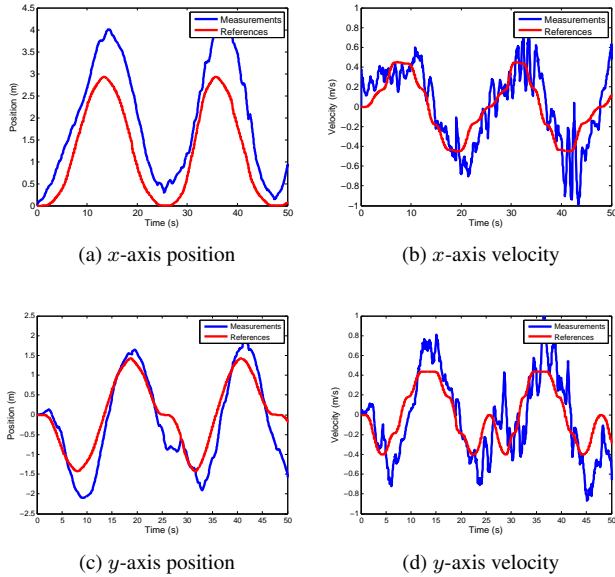


Figure 10: Tracking performance along x and y axes of the circular path

a circle with 2 m radius is then generated for the MAV to follow. It can be seen in Fig. 10, the MAV tracked the path well with no delays in both position and velocity. As there are several overshoot and drifting error in positions and oscillation in velocities for both square and circular paths, some possible causes are investigated as below:

1. Errors from scale factor. To accurately estimate the x and y axis velocity and position, the height of the MAV needs to be fixed at a certain altitude to obtain a precise scale factor. It can be seen in Fig. 9, the controlled height has noise and error up to 0.1 m compared with the set-point 0.75 m. As the height measurement from the ultrasonic sensor is not transmitted to GCS (no Wi-Fi module is developed for this platform considering the weight and computational load), the height channel errors are reflected by the errors of x and y axis due to the fixed scale in GCS. Furthermore, as the attitude measurement from IMU cannot be sent to GCS either, images are not rectified based on current attitude.
2. Severe noise in images due to signal interference causes error in the vision-based motion estimation. As stated in Fig. 5, images transmitted by analog transceiver are subject to interference and motion blur, which cause errors in feature matching for optical flow method. These problems become more severe when the transmission is blocked between the MAV and the receiver. Moreover, the optical flow method is subject to drifting error in position estimation even for clear and relatively high resolution images. Thus, it can be seen

that there are overshoot and drift error in both cases.

3. Errors from the platform. Fig. 8a and 8c shows a delay of response and an offset with respect to the reference around 2 seconds. Latency introduced by transmission from onboard analog camera to ground control station as well as image processing may cause delay in response of MAV. Further, the rotational rates of the brushed motors cannot be very precisely controlled by a chopper circuit ESC, oscillations in MAV motions are thus introduced. Also temperature rise may cause changes in the motor model, the MAV will have severe oscillations when operating for a certain period.

6 CONCLUSION

This paper presented the autonomous control design of a quadrotor MAV with regard to its hardware and software development. Based on the previous work of the ultra-light platform design as well as mathematical modeling and control, the platform equipped with a miniature ultrasonic range finder and a micro self-powered video system is capable of pre-planned trajectory tracking in an indoor environment based on visual odometry. A model based RPT control method is applied to global position control. In the current stage, we are still tuning the parameters of inner and outer loop control law to improve the control performance. In future, we aim at autonomous navigation of the MAV using 3-D vision based localisation and mapping algorithms.

REFERENCES

- [1] S. Shen, M. Nathan, and V. Kumar. Autonomous multi-floor indoor navigation with a computationally constrained mav. In *International Conference on Robotics and automation*, pages 20–25, Shanghai, China, 2011.
- [2] V. Lippiello, G. Loianno, and B. Siciliano. Mav indoor navigation based on a closed-form solution for absolute scale velocity estimation using optical flow and inertial data. In *50th IEEE Conference on Decision and Control and European Control Conference*, pages 3566–3571, Orlando, FL, USA, 2011.
- [3] S. Zingg, D. Scaramuzza, S. Weiss, and R. Siegwart. Mav navigation through indoor corridors using optical flow. In *IEEE International Conference on Robotics and Automation*, pages 3361–3368, Anchorage, AK, USA, 2010.
- [4] R. J. Wood, S. Avadhanula, M. Seeman and J. Entwistle E. Steltz, A. Bachrach, G. Barrows, and S. Sanders. An autonomous palm-sized gliding micro air vehicle. *Robotics & Automation Magazine*, 14(2):82–91, 2007.
- [5] F. M. Benjamin and R. J. Wood. Open-loop roll, pitch and yaw torques for a robotic bee. In *IEEE/RSJ International Conference on Intelligent Robots and Systems (IROS)*, pages 113–119, Vilamoura, Portugal, 2012.

- [6] J. J. Gibson. *The Ecological Approach to Visual Perception*. Lawrence Erlbaum Associates, Boston, 1986.
- [7] W. Ding, J. Wang, S. Han, A. Almagbile, M. A. Garratt, A. Lambert, and J. J. Wang. Adding optical flow into the gps/ins integration for uav navigation. In *International Global Navigation Satellite Systems Society Symposium*, pages 1–13, 2009.
- [8] M. Achtelik, S. Weiss, and R. Siegwart. Onboard imu and monocular vision based control for mavs in unknown in-and outdoor environments. In *IEEE International Conference on Robotics and automation (ICRA)*, pages 3056–3063, Shanghai, China, 2011.
- [9] F. Fraundorfer, L. Heng, D. Honegger, G. H. Lee, L. Meier, P. Tanskanen, and M. Pollefeys. Vision-based autonomous mapping and exploration using a quadrotor mav. In *IEEE/RSJ International Conference on Intelligent Robots and Systems (IROS)*, pages 4557–4564, Vilamoura, Portugal, 2012.
- [10] F. Ruffier and N. Franceschini. Visually guided micro-aerial vehicle: automatic take off, terrain following, landing and wind reaction. In *IEEE International Conference on Robotics and Automation (ICRA)*, volume 14, pages 2339–2346, New Orleans, USA, 2012.
- [11] G. de Croon, M. A. Groen, C. De Wagter, B. Remes, R. Ruijsink, and B. W. van Oudheusden. Design, aerodynamics and autonomy of the delfly. *Bioinspiration & biomimetics*, 7(2):1–36, 2012.
- [12] K. Li, S. K. Phang, B. M. Chen, and T. H. Lee. Platform design and mathematical modeling of an ultralight quadrotor micro aerial vehicle. In *International Conference on Unmanned Aircraft Systems*, pages 1077–1086, Atlanta, GA, USA, 2013.
- [13] G. Klein and D. W. Murray. Parallel tracking and mapping for small ar workspaces. In *International Symposium on Mixed and Augmented Reality (ISMAR)*, pages 225–234, Nara, Japan, 2007.
- [14] J. Shi and C. Tomasi. Good features to track. In *IEEE Conference on Computer Vision and Pattern Recognition*, pages 593–600, Seattle, WA, USA, 1994.
- [15] B. D. Lucas and T. Kanade. An iterative image registration technique with an application to stereo vision. In *International Joint Conference on Artificial Intelligence*, volume 81, pages 674–679, Vancouver, BC, Canada, 1981.
- [16] Y. Ma, S. Soatto, J. Kosecka, and S. S. Sastry. *An Invitation to 3-D Vision*. Springer, New York, NY, 2004.
- [17] M. A. Fischler and R. C. Bolles. Random sample consensus: a paradigm for model fitting with applications to image analysis and automated cartography. *Communications of the ACM*, 24(6):381–395, 1981.
- [18] R. I. Hartley and A. Zisserman. *Multiple View Geometry in Computer Vision*. Cambridge University Press, 2004.
- [19] S. K. Phang, K. Li, K. H. Yu, B. M. Chen, and T. H. Lee. Systematic design and implementation of a micro unmanned quadrotor system. *Unmanned Systems*, 2(2):121–141, 2014.
- [20] G. Cai, B. M. Chen, and T. H. Lee. *Unmanned Rotorcraft Systems*. Springer, New York, NY, 2011.
- [21] B. Wang, X. Dong, B. M. Chen, T. H. Lee, and S. K. Phang. Formation flight of unmanned rotorcraft based on robust and perfect tracking approach. In *American Control Conference*, pages 3284–3290, Montreal, QC, 2012.
- [22] B. M. Chen. *Robust and H_∞ Control*. Springer, New York, NY, 2000.
- [23] F. Wang, K. Wang, S. Lai, S. K. Phang, B. M. Chen, and T. H. Lee. An efficient uav navigation solution for confined but partially known indoor environments. In *11th IEEE International Conference on Control & Automation*, 2014 (to appear).
- [24] S. K. Phang, S. Lai, F. Wang, M. Lan, and B. M. Chen. UAV calligraphy. In *Proceedings of the 11th IEEE International Conference on Control & Automation*, pages 422–428, Taichung, Taiwan, 2014.
- [25] C. de Boor. *A Practical Guide to Splines*. Springer-Verlag, New York, NY, 1978.
- [26] H. Kano, H. Fujioka, and C. F. Martin. Optimal smoothing and interpolating splines with constraints. *Applied Mathematics and Computation*, 5(218):1831–1844, 2001.